

Supporting Information

Deciphering the multifaceted role of oleic acid in synthesizing multibranched cobalt ferrite nanoparticles with enhanced magnetic properties

Kingsley Poon^{a}, Gurvinder Singh^{a*}*

^aSchool of Biomedical Engineering, The University of Sydney, Sydney 2050, Australia

*Corresponding authors: kipo0860@uni.sydney.edu.au, and gurvinder.singh@sydney.edu.au

S1. Methods and Materials

Chemicals: 1-octadecene (technical grade, 90%), eicosane (99%), cobalt (II) chloride hexahydrate (98%), iron (III) chloride hexahydrate (Ph. Eur., $\geq 99\%$), oleic acid (90%), oleylamine (technical grade) and trimethylamine N-oxide (95%) were purchased from Sigma Aldrich. Sodium Oleate (97%) was purchased from TCI Chemicals.

Synthesis of Fe-Co Oleate: In a typical synthesis, 3.17 g cobalt (II) chloride hexahydrate, 7.19 g iron (III) chloride hexahydrate, and 32.47 g sodium oleate was dissolved into a mixture of 60 mL water, 80 mL ethanol and 140 mL hexane. The solution was heated to 70 °C and left to react overnight. To remove the excess dissolved salts and unreacted sodium oleate, the aqueous fraction was removed, and the organic fraction was diluted with ethanol. Water was then added in excess to remove the ethanol. The organic fraction was washed 3 times before the organic solvents were removed by a rotary evaporator (85 °C, 100 mbar, 3 hours).

Synthesis of 88 nm octapod NPs: 1.36 g Fe-Co Oleate was dissolved into 9.75 g 1-octadecene and 7.6 g oleic acid. The solution was slowly heated (3 °C/min) to 325 °C under an Ar environment and left to react for 5 hours with constant magnetic stirring. At the conclusion of the reaction, the NPs were precipitated using toluene and acetone. For the synthesis of octapod-like and multibranch nanoclusters, 1.65 g Fe-Co oleate and 200 mg sodium oleate was dissolved into 19.25 g eicosane. The solution was slowly heated (3 °C/min) to 335 °C under an Ar environment and left to react for 30 minutes with constant magnetic stirring. At the conclusion of the reaction, the NPs were precipitated using hexane and acetone. Hexane and ethanol were used to remove the excess sodium oleate. To investigate the effect of oleylamine on CFO octapod formation, 1.36 g Fe-Co oleate was dissolved into 9.75 g 1-octadecene and 7.2 g oleylamine or 9.75 g 1-octadecene and varying molar ratio of oleic acid: oleylamine (0.7 and 1.4).

Post-synthesis oxidation: To remove the phase impurities, 10 mg of NPs and 10 mg of trimethylamine N-oxide was dissolved into 10 mL 1-octadecene. The temperature was then quickly (10 °C/min) raised to 130 °C and left to react for 1 hour. The temperature was then raised again to 280 °C and left to react for an additional 48 hours. The NPs were precipitated using toluene and acetone.

Characterization: Low-resolution TEM images were captured using the Tecnai T12 operating at an accelerating voltage of 120 kV. X-ray powder diffraction data from the spinning samples were collected in Bragg-Brentano geometry on a Rigaku Smartlab SE powder diffractometer

equipped with a Cu $K\alpha$ X-ray source ($K\alpha_1 = 1.540598 \text{ \AA}$, $K\alpha_2 = 1.544426 \text{ \AA}$) operating at 40 kV and 40 mA, a 10 mm length-limiting slit and $\frac{1}{4}^\circ$ divergence slits. Diffraction data were collected using an XSPA-400 ER two-dimensional detector scanning continuously at $1.5^\circ/\text{min}$ over the 2θ angle range $20\text{--}70^\circ$. The magnetic properties were measured using the Dynacool Physical Properties Measurement System (PPMS) with a vibrating sample magnetometer (VSM). The hysteresis loops were measured by sweeping the field from -90 kOe to $+90 \text{ kOe}$. Field-cooled and zero field-cooled curves were measured under a 100 Oe applied field.

High-Resolution TEM: TEM images were collected on a Thermofisher Themiz Z aberration-corrected TEM at 300 kV accelerating voltage. The EELS spectrum images for mapping were collected with a collection angle of 69 mrad and a screen current of 100 pA . 60 \mu s dwelling time was used for efficiency. Gatan Microscopy Suite 3.5 was used for data analysis.

S2. HAADF-STEM images of CFO octapod NPs

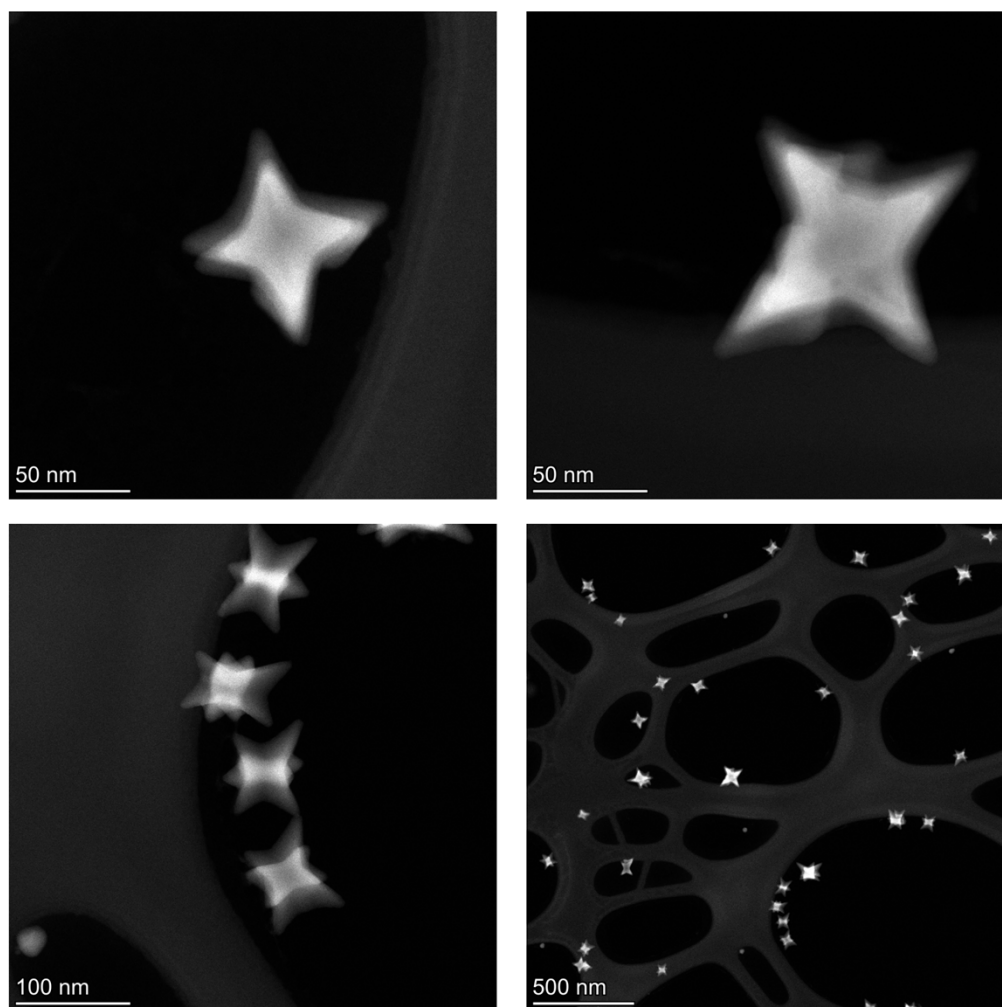


Fig. S1 HAADF-STEM images of octapod NPs highlight the distinct octapod morphology, with eight symmetrical arms radiating from the nanoparticle core.

S3. High index facets enclosed by CFO octapod NPs

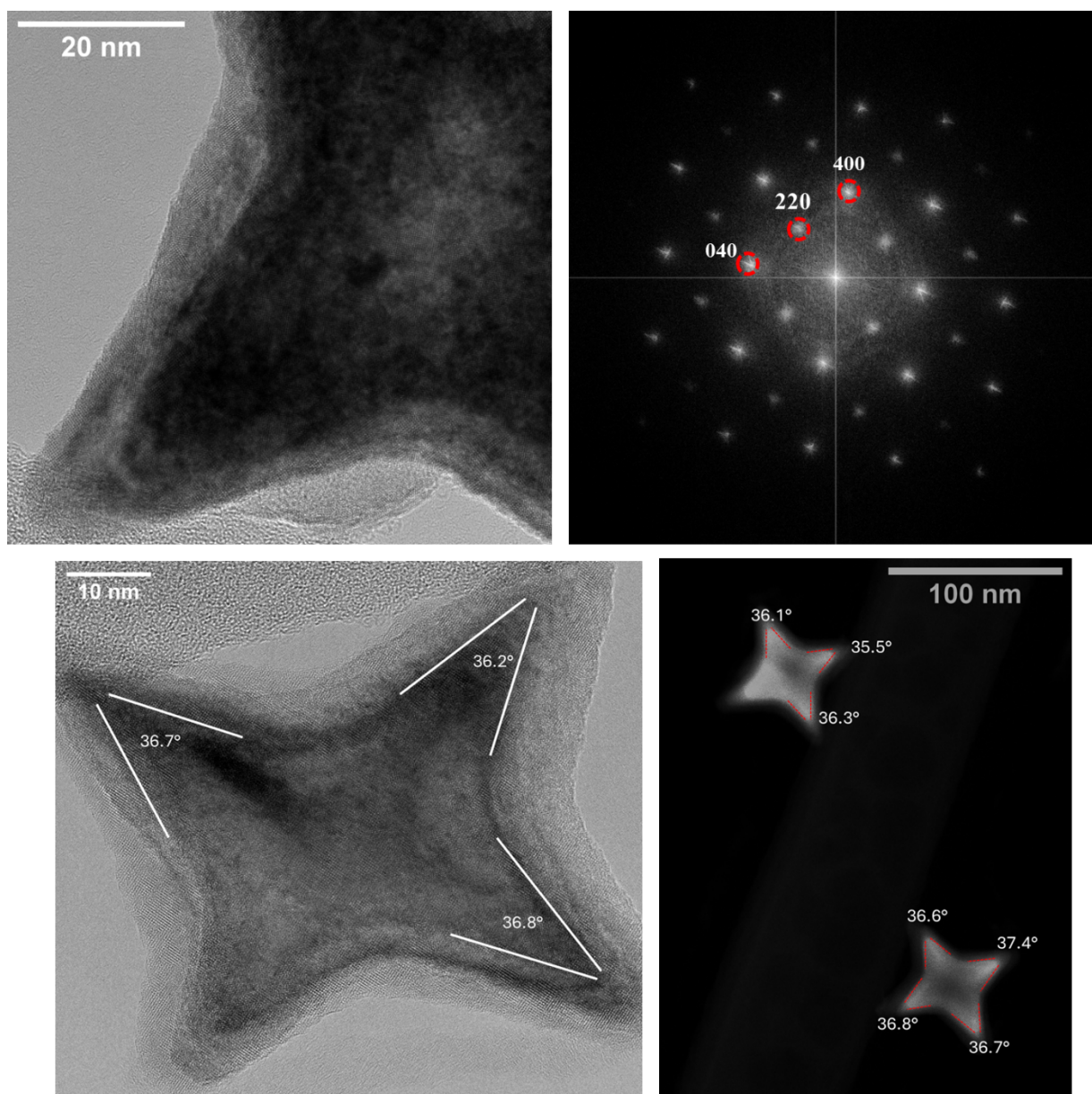


Fig. S2 HRTEM image of octapod arm (left upper panel) and the corresponding FFT pattern (right upper panel) along [001] zone axis. The white lines denote the locations where apex angle measurements were performed on the octapod arms in HRTEM and STEM-HAADF images.

S4. Magnetic characterization of octapod NPs

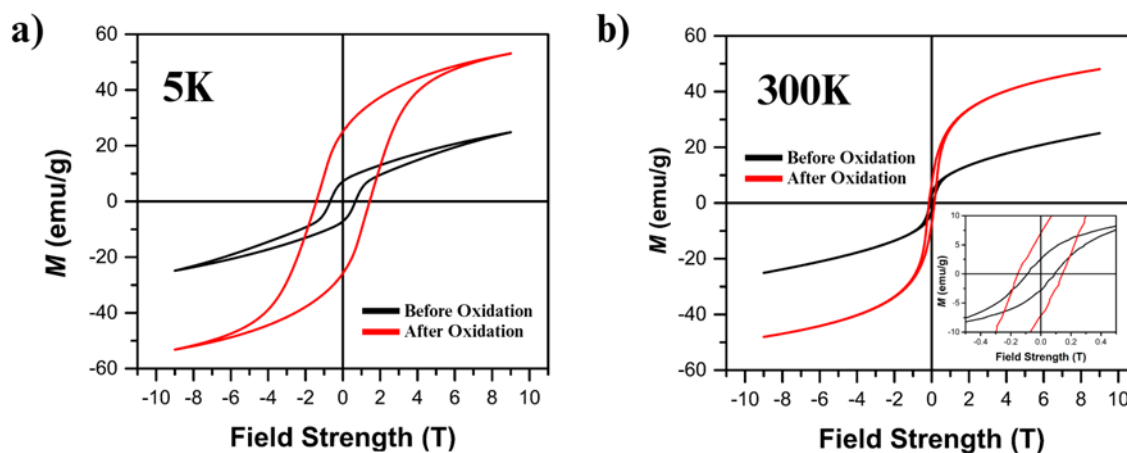


Fig. S3 a, b) Hysteresis loops as measured before and after oxidation at 5 and 300K, prior to subtraction of the paramagnetic contribution.

S5. Octapod synthesis using iron (III) oleate

Using a similar synthetic protocol that used for the fabrication of CFO octapod NPs, we demonstrated the synthesis of iron oxide octapod NPs using iron (III) oleate. During the reaction, we observed a comparable shape progression, wherein intermediate morphologies, such as cuboctahedra and cubic nanoparticles, emerged before evolving into fully developed octapods, followed by their transformation into concave cubes and polyhedral NPs.

Ageing time

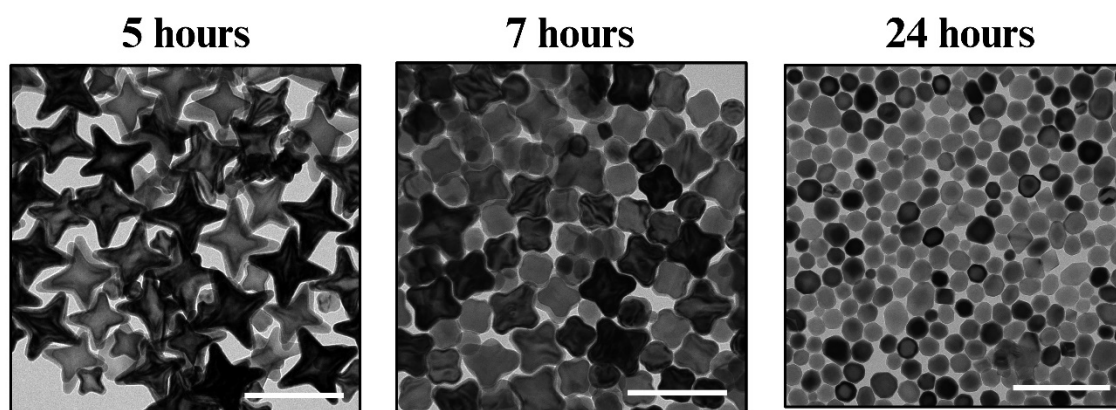


Fig. S4 NP synthesised using iron (III) oleate follows an identical shape progression as those synthesized using Fe-Co Oleate. Scale bar represents 200 nm.

S6. Volume approximation of anisotropic magnetic NPs

Because the volume of an octapod NP cannot be easily estimated, the volumetric differences between the morphologies observed from 5 hours (octapod) to 16 hours (cuboctahedra) can be estimated by measuring the NP "body size". The "body" of the NP for cubic- and octapod-like NP represents the largest fitting cuboid within the 3D geometry. The cuboid can be estimated by drawing the largest rectangle within the NP and measuring the dimensions (a and b). For an octapod, the cuboid represents the minimum volume of the NP by excluding the volume of the octapod arms. For blunted octapods/cube (*i.e.* NPs observed at 12 hours), the cuboid has an approximate equivalent volume. The volume of the cuboctahedra can be estimated by the largest ellipsoid with equivalent dimensions to the NP. The third dimension for all the shapes is assumed to have a length equal to the average of the a and b (Fig. S5). Therefore, for the same linear dimensions between these shapes (*i.e.*, $a_{\text{octapod}} = a_{\text{cuboid}} = a_{\text{ellipsoid}}$ *etc.*), $V_{\text{octapod}} > V_{\text{cuboid}} > V_{\text{ellipsoid}}$.

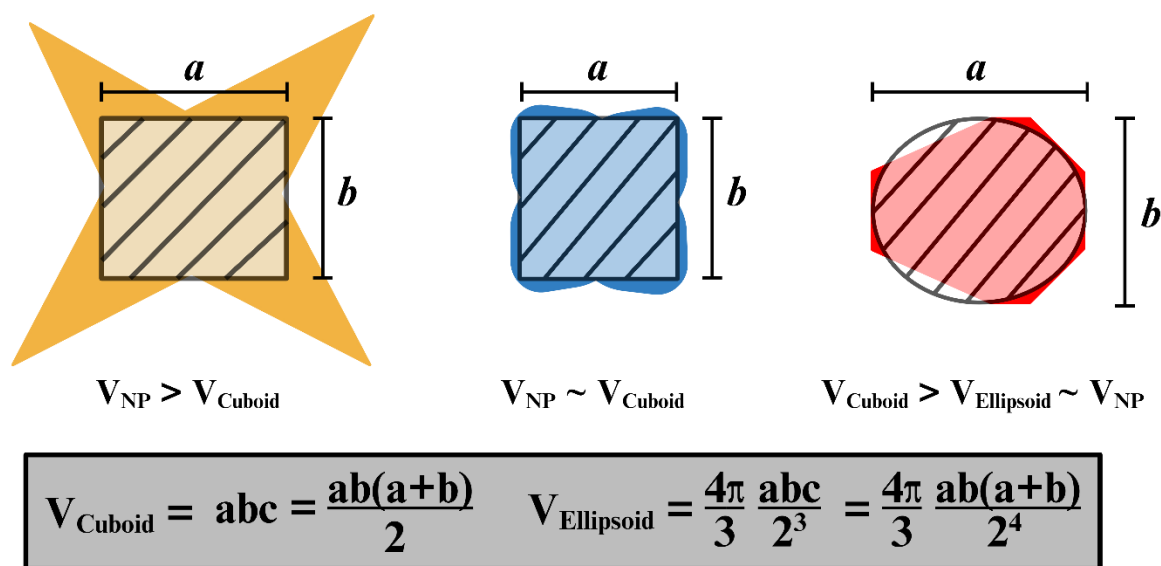


Fig. S5 Approximation of the octapod, cubic-like, and polyhedral NP volume based on their measured linear dimensions. The cuboid volume represents the minimum volume of the octapod and the maximum volume of the ellipsoid.

Fig. S6 shows the change in average NP volume of samples taken at various time points, calculated using the “body size. The volume distribution of NP samples taken during the latter half of the reaction is also presented in Fig. S6. If atomic diffusion from the octapod arms to the NP body and edges is the origin of the shape transformation, then the measured “body size” should increase with reaction time. However, $V_{5 \text{ hours}} > V_{12 \text{ hours}} > V_{16 \text{ hours}}$, suggesting the dissolution of atoms from the NP during the aging time. Moreover, the volumetric differences between the bimodal distribution increases over time, consistent with the initial dissolution of smaller NPs with higher surface energy.

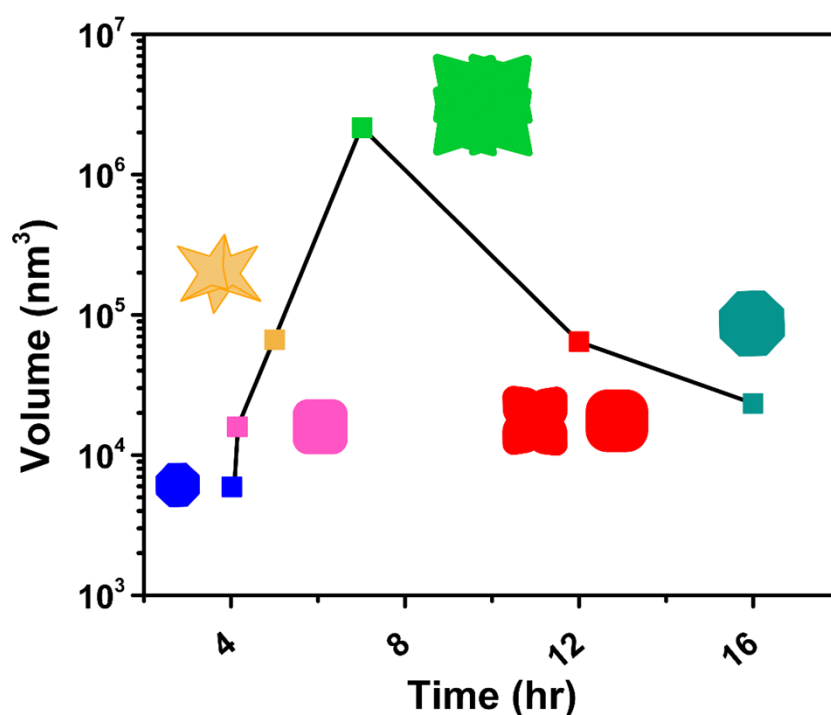


Fig. S6. Volumetric change of NPs at different timepoints throughout the reaction, as calculated using the “body size”.

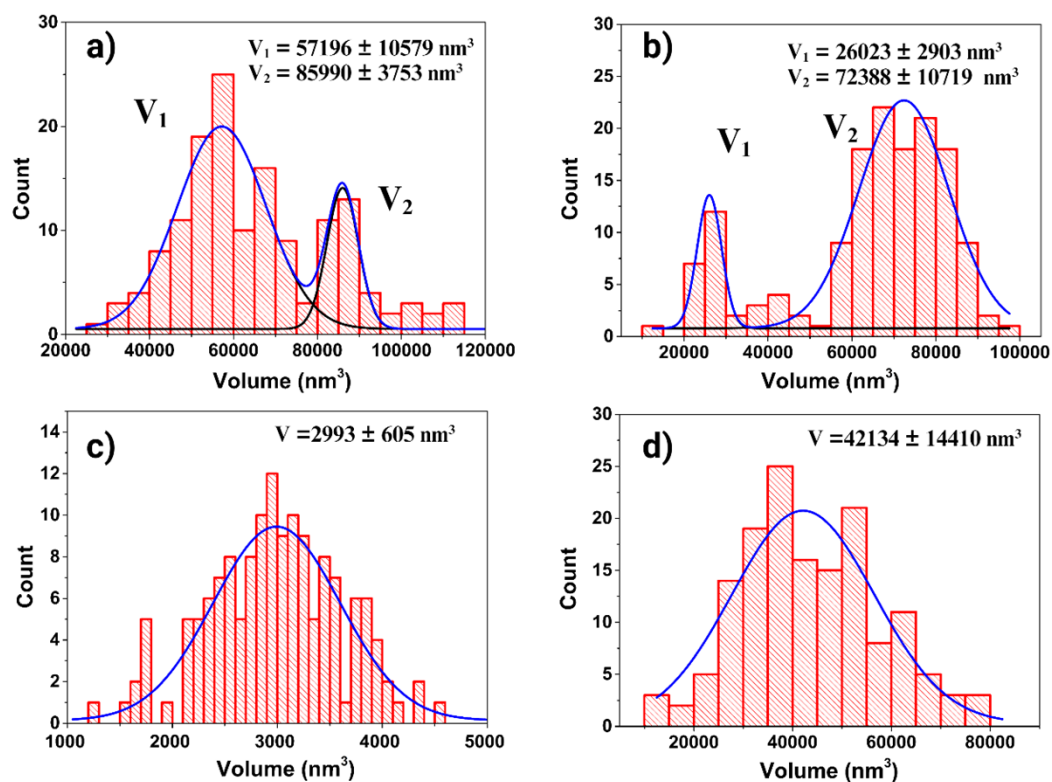


Fig. S7 Volume distribution of the synthesized NPs based on the octapod, cuboid, and ellipsoid model. The volumes were calculated at various time points: a) 5 hours, b) 12 hours, c, d) 16 hours (n = 150).

S7. Role of OA in the morphological regression of cubic CFO NPs

In the absence of OA in the growth solution, CFO NPs retain their original morphology even at elevated temperature, indicating their intrinsic structural stability in the absence of surfactants. However, when OA is introduced, the cubic shaped CFO NPs gradually undergo shape transformation over time, suggesting that OA promotes the regression of cubic morphology through a dynamic process of OA induced dissolution and redeposition.

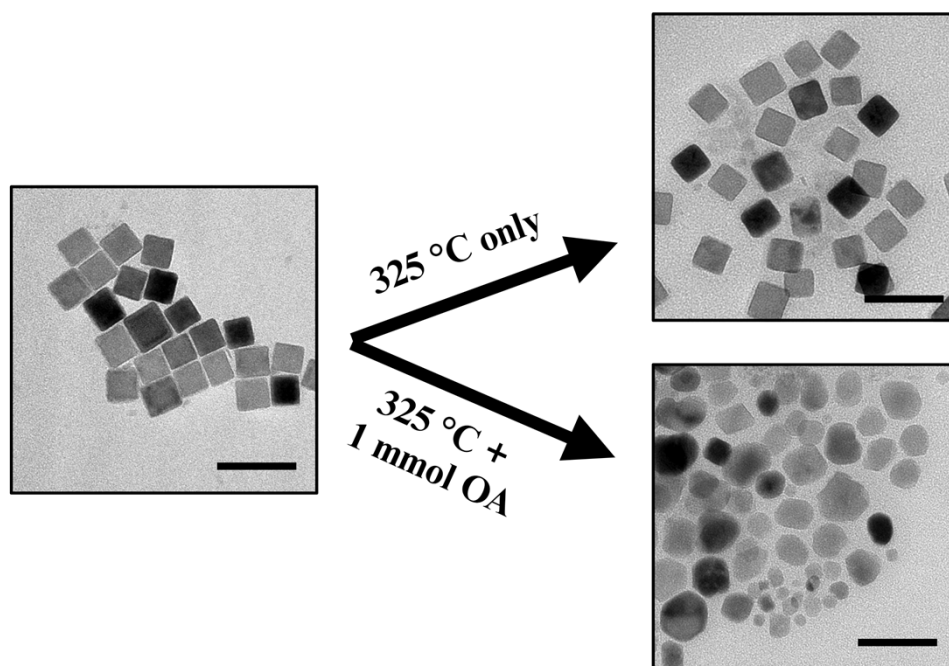


Fig. S8 Cubic CFO NP regression in the present of OA. The retention of the cubic shape in the absence of OA further demonstrates the same intrinsic stability as octapod NPs.

S8. Additional TEM images showing morphological evolution of CFO NPs at reduced OA and solvent (ODE)

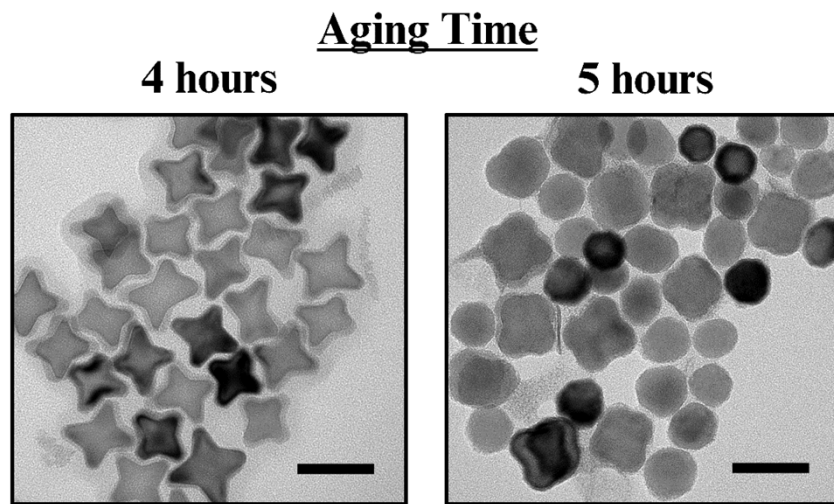


Fig. S9 TEM images of octapod NPs synthesised with a reduced OA concentration (Fe-Co Oleate: OA ~50) and ODE volume (4.9 g). Small octapod NPs appear at an earlier time point with high shape purity (left panel) and their transformation to concave/polyhedral shape NPs (right panel). Scale bar represents 50 nm.

S9. Influence of OA Purity on the Synthesis of Octapod NPs

The synthesis of octapod NPs using OA from different sources reveals distinct variations in reaction dynamics, likely due to differences in the chemical purity of the surfactant. These discrepancies in OA purity can affect key factors such as ligand binding strength, monomer deposition rate, and crystal facet stabilization, ultimately influencing the growth and morphology of the NPs.

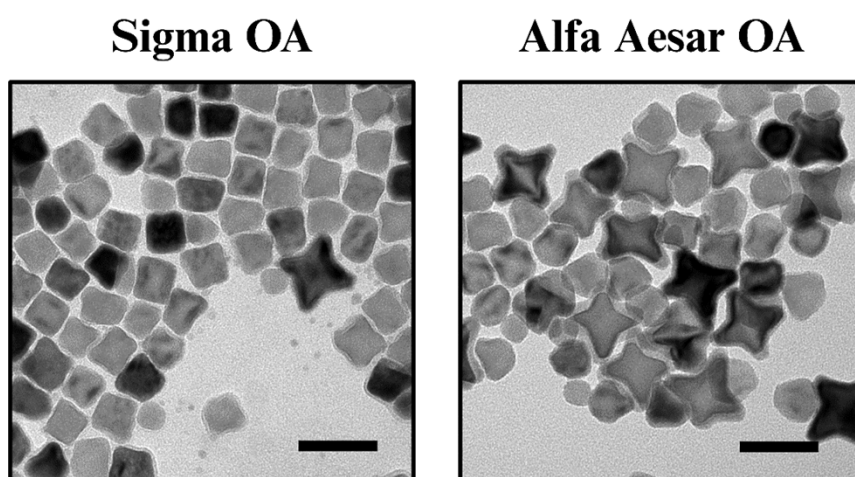


Fig. S10 Octapod NPs synthesised with OA from different sources. There is a noticeable difference in the reaction dynamics that might be attributed to the chemical purity of the OA. Scale bar represents 50 nm.

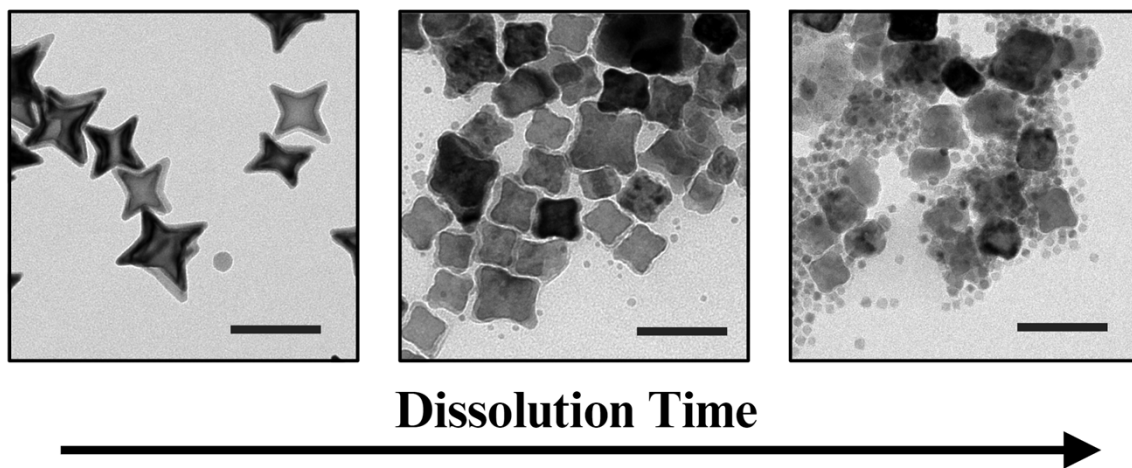
S10. Decomposition of OA at high temperatures

Fig. S10 shows the thermal decomposition of oleic acid (OA) during the NP synthesis process. As the temperature rises, a noticeable discoloration of the synthesis solution occurs, accompanied by a decrease in the reaction temperature to approximately 240 °C in the absence of metal oleate. This change in color and temperature signifies the breakdown of oleic acid, highlighting its instability at high temperatures. The findings emphasize the importance of maintaining optimal conditions during synthesis to prevent the degradation of surfactants, which can impact the morphology and stability of the resulting NPs.



Fig. S11 Discolouration of the synthesis solution and drop in reaction temperature (~240 °C) in the absence of metal oleate is indicative of oleic acid breakdown.

S11. Effect of dissolution time on octapod NPs in the presence of OA



F

ig. S12 Octapod arm length can be tuned by varying the OA concentration, reaction temperature, or dissolution time.

S12. Effect of OAm and ratio of OA:OAm on NP morphology

To further investigate the role of OAm in octapod formation, control experiments were performed under identical conditions by introducing OAm alone (~34 mmol) and in combination with OA at both low and high OA:OAm molar ratio (0.7 and 1.4). In all cases, we observed polyhedral or spherical morphologies of NP, with no evidence of octapod NP (Fig. S12). These results suggest that OAm, whether used alone or together with OA at varying molar ratios, does not facilitate octapod NP formation. This finding further supports the critical role of OA in directing the anisotropic NP growth required for the evolution of CFO octapod NP.

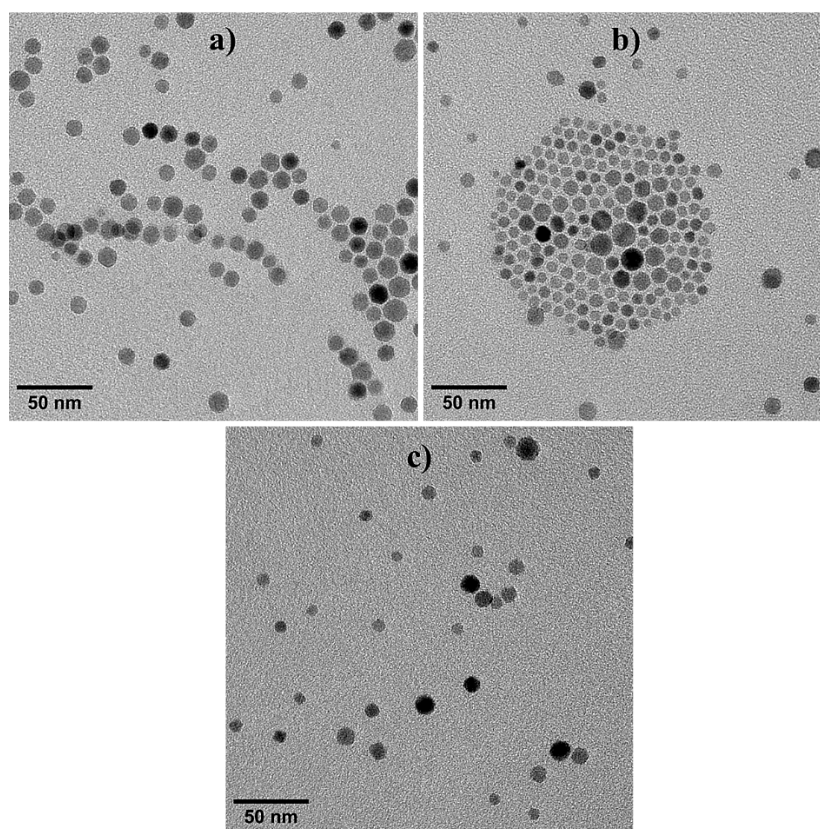


Fig. S13 TEM images showing the effect of OAm and varying OA:OAm molar ratio on NP morphology. a) NP synthesized with OAm only, b) a low OA:OAm molar ratio (0.7) and c) a high OA:OAm molar ratio (1.4) showed polyhedral or spherical morphologies of NP.